Int. J. Heat Mass Transfer. Vol. 36, No. 10, pp. 2479–2498, 1993
Printed in Great Britain

0017-9310/93 $6.00+0.00

On natural convection in vertical porous enclosures due to prescribed fluxes of heat and mass at the vertical boundaries†

FARID ALAVYOON‡

Government Industrial Research Institute, Tohoku, Agency of Industrial Science and Technology, Ministry of International Trade and Industry, Nigatake, 4-2-1, Miyagino-Ku, Sendai, 983, Japan

(*Received* 16 *September* 1992 *and in final form* 6 *January* 1993)

Abstract—Unsteady and steady convection in a fluid-saturated, vertical and homogeneous porous enclosure has been studied numerically on the basis of a two-dimensional mathematical model. The buoyancy forces that induce the fluid motion are due to cooperative and constant fluxes of heat and mass on the vertical walls. For the steady state, an analytical solution, valid for stratified flow in slender enclosures, is presented. Scale analysis is applied to the two extreme cases of heat-driven and solute-driven natural convection. Comparisons between the fully numerical and analytical solutions are presented for $0.1 \leqslant R_c \leqslant 500$, $2 \leqslant Le \leqslant 10^2$, $10^{-2} \leqslant N \leqslant 10^4$ and $1 \leqslant A \leqslant 10$, where R_c, Le, N and A denote the solutal Rayleigh–Darcy number, Lewis number, inverse of buoyancy ratio and enclosure aspect ratio, respectively. The numerical results show that for any value of $Le > 1$, there exists a minimum A below which the concentration field in the core region is rather uniform and above which it is linearly stratified in the vertical direction. For sufficiently high aspect ratios, the agreement between the numerical and analytical solutions is good. The results of the scale analysis agree well with approximations of the analytical solution in the heat-driven and solute-driven limits. The numerical results indicate that for $Le > 1$ the thermal layers at the top and the bottom of the enclosure are thinner than their solutal counterparts. In the boundary layer regime, and for sufficiently high A, the thicknesses of the vertical boundary layers of velocity, concentration and temperature are shown to be equal, regardless of the value of Le.

1. INTRODUCTION

THIS PAPER reports a theoretical study of transient and steady-state double diffusive natural convection in a fluid-saturated rectangular porous enclosure. Fluid motion is caused by buoyancy forces which, in turn, are due to the prescription of constant and cooperative gradients of temperature and concentration on the vertical walls of the enclosure. The main purpose of this work is to present a steady-state analytical solution valid for a wide range of input parameter values.

Natural convection due to spatial variations of fluid density is of fundamental importance in many natural and industrial problems. It can occur in free bodies of fluid as well as in porous media. The variation of fluid density can be due to nonuniform distribution of temperature and/or concentration of a dissolved substance. Some examples of heat and/or solute transfer by natural convection can be found in: thermal insulation engineering, solar power collectors, reactor cooling systems, underground disposal of wastes, spreading of pollutants, oceanography, geophysics, astrophysics, metallurgy and electrochemistry. Most of the reported surveys on natural convection deal with cases in which the buoyancy forces are due to the variations of only one component, namely either temperature or solute concentration. The interest of research in the more complicated and neglected case of flow due to variations of several components has, perhaps due to its importance in environmental and energy related problems, increased significantly during recent years. Such phenomena are usually referred to as thermohaline, double diffusive (adopted in this paper) or combined heat and mass transfer natural convection. Since the different components of a fluid, such as temperature and solute concentration, diffuse at widely different rates, double diffusive phenomena often exhibit special features, such as fingering and layering, that lack counterparts in single-component cases, see refs. [1] and [2]. In mathematical investigations of double diffusive phenomena, the assumption that different components have the same diffusivity, i.e. $Le = 1$, relates them in such a way that suppresses any tendency of the mathematical model to reveal the exclusive features of double diffusive convection [2]. However, in most of the theoretical investigations available in the literature, a relatively large part of the reported results deal with the case of $Le = 1$. This is perhaps due to the computational economy, in numerical works, and the algebraic convenience, in analytical works, that such an assumption leads to.

Isosolutal, or isothermal, buoyancy-driven convection in rectangular porous enclosures subject to

† Dedicated to Professor Fritz H. Bark on the occasion of his 50th birthday (December 1992).

‡ Present address: Vattenfall Utveckling AB, S-810 70 Älvkarleby, Sweden.

NOMENCLATURE

A	aspect ratio
br	buoyancy ratio, $(\beta\Delta c)/(\alpha\Delta T)$
c	concentration
d	horizontal length scale
D	solute diffusivity
g	acceleration of gravity
$2h$	enclosure width
$2H$	enclosure height
k	permeability
$\mathscr{L}$	vertical length scale
Le	Lewis number
N	inverse of buoyancy ratio, $1/br$
Nu	Nusselt number
P	pressure
R	Rayleigh–Darcy number
S	absolute value of vertical gradient
Sh	Sherwood number
t	time
T	temperature
$\mathbf{u}$	velocity vector, (u, v)
$\mathscr{V}$	velocity scale
x	horizontal coordinate
y	vertical coordinate.

Greek symbols

α	coefficient of thermal expansion
β	coefficient of concentration expansion
δ	boundary layer thickness
Δc	typical concentration variation
ΔT	typical temperature variation
ε	porosity
θ	nondimensional concentration variation
κ	thermal diffusivity
Λ	horizontal gradient prescribed on the side wall
μ	viscosity
ν	horizontal profile
ρ	density
σ	heat capacity ratio
φ	nondimensional temperature variation
ψ	stream function.

Subscripts and superscripts

c	solutal
T	thermal
0	initial.

prescribed gradients of temperature, or concentration, on the side walls has been studied numerically and analytically by, among others, Bejan [3], Vasseur *et al.* [4, 5], and Alavyoon [6]. Based on similar mathematical procedures, analytical boundary layer solutions were derived and presented for steady convection in a slender cavity, [4–6]. The analytical solutions were verified by comparison with fully numerical solutions. The main conclusions reported in [4–6] are that, in the high Rayleigh–Darcy regime of flow, (i) the core region is motionless, (ii) the boundary layers have constant thicknesses, and (iii) the density field is linearly stratified in the vertical direction. In two reports, Bark *et al.* [7] and Alavyoon *et al.* [8], presented simplified perturbation models for time-dependent natural convection in fluid-filled slender cavities. These models were verified by both fully numerical calculations and electrochemical experiments. The time-dependent perturbation solutions presented in refs. [7, 8] were extended to porous media by Alavyoon [6].

Theoretical investigations of double diffusive natural convection in porous media have been reported for a variety of geometrical configurations (external or internal flows) and boundary conditions (prescribed values of the components or their derivatives on solid boundaries), see e.g. refs. [9–17]. Bejan and Khair [9] reported an analytical investigation of double diffusive natural convection near a vertical surface immersed in an infinite porous medium. Constant temperature and concentration values were prescribed on the vertical surface. Scale analysis was applied to the two extreme cases of heat-driven and solute-driven natural convection in order to derive the order of magnitude of the properties of interest. A boundary layer similarity solution was presented for $-5 \leqslant br \leqslant 4$, and $1 \leqslant Le \leqslant 100$, excluding the interval $-1 < br < 0$ for $Le = 1$. The similarity solution supported the results of the scale analysis, see ref. [9]. In a more recent paper, Lai and Kulacki [10] re-examined the case studied by Bejan and Khair [9]. They [10] presented similarity solutions for the two cases of constant wall temperature and concentration, and constant wall heat and mass flux. Their results gave support to the scale analysis of Bejan and Khair [9]. Contrary to ref. [9], Lai and Kulacki [10] found a similarity solution for the case of $-1 < br < 0$ and $Le = 1$. Instead, they [10] argued that such solutions are impossible in the range of $-1 < br$. References [11–17] represent a few of the theoretical papers published during the eighties and the early nineties on internal double diffusive natural convection in rectangular porous media, which also is the subject of the present paper. Trevisan and Bejan [11], used numerical methods to study heat and mass transfer in a square cavity with isolated top and bottom and constant temperature and concentration on the vertical walls. They [11] also applied scale analysis to the heat-driven and solute-driven limits in order to, among other things, estimate the overall heat and mass transfer rates. The results of their scale analysis agreed with those of the fully numerical solution. In

ref. [12], Trevisan and Bejan presented numerical and analytical results for a fluid-saturated rectangular porous enclosure subject to constant gradients of temperature and solute concentration at the vertical walls. Based on the results of an earlier work [3], the authors [12] developed an analytical boundary layer solution to the problem. However, due to an inappropriate choice of core condition (matching the boundary layer solution to the core region solution), their analytical solution proved to be valid only for the case of $Le = 1$. Instead, for $Le > 1$, an analytical similarity solution was presented in the heat-driven limit [12]. The present paper, among other things, re-examines the first part of ref. [12]. Trevisan and Bejan [13] studied high Rayleigh–Darcy number, heat-driven double diffusive convection in a rectangular cell heated from below. The values of temperature and concentration were prescribed on the horizontal walls. The flow was driven by a destabilizing vertical gradient of temperature. Numerical experiments and scale analysis arguments were used to reveal the relationship between the temperature and concentration fields. The agreement between the two methods was good. An interesting result reported in ref. [13] was the appearance of different temperature scales in the vertical and horizontal directions. Zhang and Bejan [14] studied time-dependent buoyancy-driven spreading of heat and chemical species in a rectangular fluid-saturated porous medium bounded by isolated walls. The flow started due to an initially nonuniform distribution of temperature and solute concentration. Numerical methods and scale analysis were used, and for the case of infinitely shallow enclosure, a closed form analytical solution was proposed [14]. Mehta and Nandakumar [15] numerically studied the effect of nonuniform permeability on heat and mass transfer in a square porous cavity. The vertical walls of the cavity were subject to constant heat and solute flux and the horizontal walls were isolated. They [15] found that, due to vigorous convection in regions with high permeability, the overall Sherwood and Nusselt numbers can differ significantly from cases in which the permeability of the enclosure is uniform. In a comprehensive review article [16], Trevisan and Bejan summarized available studies on double diffusive convection. In a recently published paper [17], Rosenberg and Spera numerically investigated double diffusive natural convection in a square porous cavity heated from below and subject to a variety of solutal boundary and initial conditions. Results for steady state and transient cases were reported. Regression analysis was applied to derive parametric relationships for Nu and Sh. In the case where the cavity was salted from below, good agreement was found with the results of ref. [13].

To the knowledge of the present author, only a few experimental studies of double diffusive natural convection in porous media are available in the literature. Griffiths [18] observed a thin diffusive interface in a Hele Shaw cell and in a laboratory porous medium, and thus concluded that layered double diffusive convection can occur in porous media. Murray and Chen [19] made an experimental study of the onset of double diffusive convection in a finite box of porous medium. They [19] found good agreement between the critical Rayleigh–Darcy number of the experiments and that of a modified version of Nield's linear theory [20].

2. PROBLEM STATEMENT

A two-dimensional mathematical model is used here for investigating momentum, heat and mass transport phenomena in a vertical, slender and porous enclosure. For simplicity, all material parameters are treated as constant and uniform. The geometry of the enclosure and its dimensions, along with the boundary conditions, are given in Fig. 1(a). The cavity consists of a fluid-saturated porous medium enclosed by solid and impermeable walls. The fluid is initially homogeneous and at rest. The top and bottom walls are isolated. The gradients of temperature and solute concentration are prescribed on the vertical walls. It is assumed that these gradients are constant and uniform. Upon starting the process, horizontal gradients of temperature and concentration appear in the fluid adjacent to the vertical walls, thus giving rise to buoyancy forces that are the cause of natural convective motion in this study. The equation for conservation of momentum in the Darcy regime and with Boussinesq approximation [1]

$$\frac{\mu}{k}\mathbf{u} = -\nabla P - \rho g[\beta(c-c_0) - \alpha(T-T_0)]\bar{e}_y \quad (1)$$

and the equation of continuity

$$\nabla\cdot\mathbf{u} = 0 \quad (2)$$

are used here to model the fluid motion.

The equations for the conservation of concentration and heat, in the absence of Soret and Dufour diffusion, read [1]

$$\varepsilon\frac{\partial c}{\partial t} + \mathbf{u}\cdot\nabla c = D\nabla^2 c \quad (3)$$

$$\sigma\frac{\partial T}{\partial t} + \mathbf{u}\cdot\nabla T = \kappa\nabla^2 T \quad (4)$$

where

$$\sigma = \frac{\varepsilon(\rho C_p)_{\text{fluid}} + (1-\varepsilon)(\rho C_p)_{\text{solid}}}{(\rho C_p)_{\text{fluid}}}.$$

The boundary conditions for equations (1)–(4) are

$$\frac{\partial c}{\partial y} = 0, \quad \frac{\partial T}{\partial y} = 0 \quad \text{and} \quad v = 0 \text{ at } |y| = H \quad (5)$$

$$\frac{\partial c}{\partial x} = -\Lambda^{(c)}, \quad \frac{\partial T}{\partial x} = \Lambda^{(T)} \quad \text{and} \quad u = 0 \text{ at } |x| = h \quad (6)$$

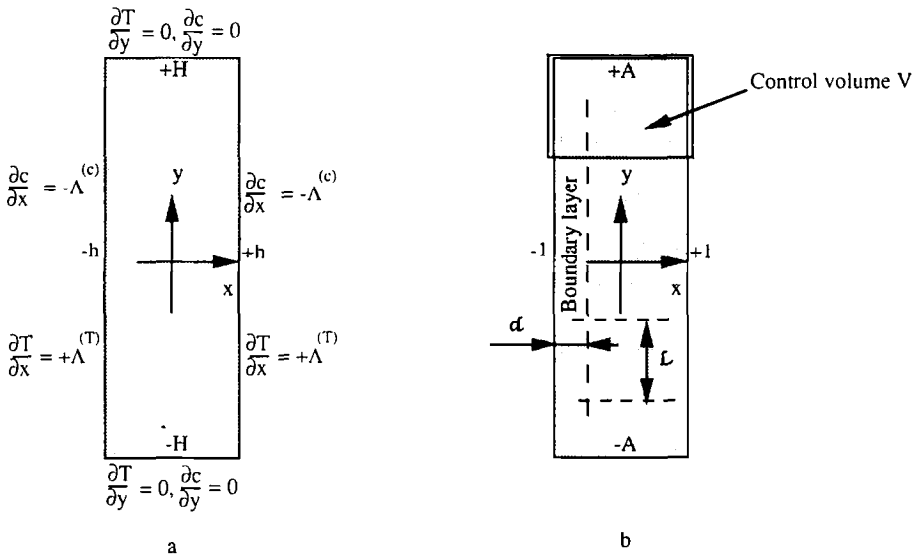

FIG. 1. The geometry of the porous enclosure. (a) Dimensions and thermal and solutal boundary conditions, (b) nondimensional form and arbitrary control volume.

where $\Lambda^{(c)} > 0$, $\Lambda^{(T)}$ is positive in the cooperating case, and negative in the opposing case. Both $\Lambda^{(c)}$ and $\Lambda^{(T)}$ are assumed to be positive and known constants here.

The initial conditions from which the process is started read

$$c = c_0, \quad T = T_0 \quad \text{and} \quad \mathbf{u} = 0 \text{ at } t = 0. \tag{7}$$

The dimensionless variables and parameters

$$x^* = \frac{x}{h}, \quad y^* = \frac{y}{h}, \quad t^* = \frac{Dt}{h^2}, \quad \mathbf{u}^* = \frac{h\mathbf{u}}{D}, \quad \theta = \frac{c-c_0}{\Lambda^{(c)}h},$$

$$\varphi = \frac{T-T_0}{\Lambda^{(T)}h}, \quad P^* = \frac{kP}{\mu D}, \quad A = \frac{H}{h}, \quad Le = \frac{\kappa}{D},$$

$$R_c = \frac{kg\beta\Lambda^{(c)}h^2}{\nu D} \quad \text{and} \quad N = \frac{\alpha\Lambda^{(T)}}{\beta\Lambda^{(c)}}$$

are used to make (1)–(7) nondimensional. Henceforth, the asterisks that denote some of the dimensionless quantities are omitted. Upon introducing the dimensionless quantities into (1)–(7), the nondimensional version of the problem to be considered reads

$$\mathbf{u} = -\nabla P - R_c(\theta - N\varphi)\tilde{e}_y \tag{8}$$

$$\nabla \cdot \mathbf{u} = 0 \tag{9}$$

$$\varepsilon\frac{\partial\theta}{\partial t} + \mathbf{u}\cdot\nabla\theta = \nabla^2\theta \tag{10}$$

$$\sigma\frac{\partial\varphi}{\partial t} + \mathbf{u}\cdot\nabla\varphi = Le\nabla^2\varphi \tag{11}$$

$$\frac{\partial\theta}{\partial y} = 0, \quad \frac{\partial\varphi}{\partial y} = 0 \quad \text{and} \quad v = 0 \text{ at } |y| = A \tag{12}$$

$$\frac{\partial\theta}{\partial x} = -1, \quad \frac{\partial\varphi}{\partial x} = 1 \quad \text{and} \quad u = 0 \text{ at } |x| = 1 \tag{13}$$

$$\theta = 0, \quad \varphi = 0 \quad \text{and} \quad \mathbf{u} = 0 \text{ at } t = 0. \tag{14}$$

In order to get rid of the pressure gradient term, one can take the curl of equation (8) and introduce the stream function ψ, defined by

$$\mathbf{u} = \left(\frac{\partial\psi}{\partial y}, \quad -\frac{\partial\psi}{\partial x}\right).$$

Thus, upon the introduction of the stream function, equations (8) and (9) get replaced by

$$\nabla^2\psi = R_c\left(\frac{\partial\theta}{\partial x} - N\frac{\partial\varphi}{\partial x}\right). \tag{15}$$

The boundary and initial conditions for the stream function are

$$\psi = 0 \text{ at } |x| = 1 \quad \text{and} \quad |y| = A \tag{16}$$

and

$$\psi = 0 \text{ at } t = 0. \tag{17}$$

Equation (15) is used only in the numerical solution to the problem.

3. NUMERICAL METHOD

The equations (10), (11) and (15) and the boundary and initial conditions (12)–(14), (16) and (17) are discretized on a rectangular mesh, uniform in each coordinate direction. There are no grid points on the physical boundaries ($|y| = A$ and $|x| = 1$). Instead, the mesh is chosen such that the first (or the last) grid points in each coordinate direction are half a length step after (or before) each physical boundary. The temporal and spacial derivatives are approximated by first- and second-order discretizations, respectively.

For simplicity, the nonlinear terms in equations (10) and (11) are evaluated by using the already known results from the last time step. Thus, three decoupled and linear systems of algebraic equations are derived. Each of these systems has a symmetric positive-definite band-matrix with constant coefficients. These algebraic systems are then solved by the conjugate gradient method [21]. The length steps, in each direction, and the time steps are chosen partly by numerical experiments and partly by the guidance provided by the analytical results of Section 5, according to which, e.g., for given values of R_c, Le and N, the thickness of the vertical boundary layer is $O(1/\Omega)$. At each new time step, the solution is deemed converged when

$$\text{Max}\left\{\frac{|\Xi_{k+1}^{n+1}-\Xi_{k}^{n+1}|}{|\Xi_{k+1}^{n+1}|}\right\} < 10^{-5}$$

where Ξ denotes any of the three quantities θ, φ or ψ. n and k denote the number of time steps and the number of iterations at each time step, respectively. The solution is assumed to have reached steady state as soon as the criterion

$$\text{Max}\left\{\frac{|\Xi^{n+1}-\Xi^{n}|}{|\Xi^{n+1}|}\right\} < e,$$

where $10^{-7} < e < 10^{-12}$, is satisfied.

The numerical method outlined here is chosen more for its simplicity than its efficiency. Partly due to the linearization of the nonlinear terms and partly due to the uniformity of the grid, this method is not suitable for cases in which R_c and/or $R_T > 10^3$. However, for the main purpose of this work, which is to verify the validity of the analytical solution discussed in Section 5, the numerical method adopted here proves to be fully sufficient. An already available Fortran code, used previously for the computations in ref. [6], is further developed and improved to conform to the numerical method outlined in this section. The code is then verified by an analytical solution valid for small values of time, see Section 4. The program was run on a Titan 750 super workstation. The numerical results presented here (typically 5000 mesh points and $\Delta t \sim 10^{-5}$), depending on the aspect ratio and values of input parameters, took approximately $3 \sim 5$ CPU hours each.

4. ANALYTICAL SOLUTION FOR SMALL VALUES OF TIME

For sufficiently small values of time and large aspect ratios, one can assume that the solution to the problem has the following form

$$\mathbf{u} = v(x,t)\bar{e}_y, \quad \theta = \theta(x,t) \quad \varphi = \varphi(x,t)$$
$$\text{and} \quad P = f(t)y. \tag{18}$$

The expressions in (18) imply that, for sufficiently small values of t, the vertical gradients of concentration and temperature are negligible, the end effects due to the presence of the horizontal walls at the top and bottom are confined to small regions there and the transport of solute and heat is diffusion-dominated. Introducing (18) into the equations (8)–(11) gives

$$v = -f - R_c(\theta - N\varphi) \tag{19}$$

$$\varepsilon\frac{\partial\theta}{\partial t} = \frac{\partial^2\theta}{\partial x^2} \tag{20}$$

$$\sigma\frac{\partial\varphi}{\partial t} = Le\frac{\partial^2\varphi}{\partial x^2}. \tag{21}$$

Equations (20) and (21), together with boundary conditions (13) can be solved by, e.g., the method of Laplace transforms. The solutions for concentration and temperature then read

$$\theta = -x - \frac{8}{\pi^2}\sum_{n=0}^{\infty}\frac{(-1)^{n+1}}{(2n+1)^2} \times \sin\left[(2n+1)\frac{\pi}{2}x\right]\exp\left(-\frac{(2n+1)^2}{4\varepsilon}\pi^2 t\right) \tag{22}$$

$$\varphi = x + \frac{8}{\pi^2}\sum_{n=0}^{\infty}\frac{(-1)^{n+1}}{(2n+1)^2} \times \sin\left[(2n+1)\frac{\pi}{2}x\right]\exp\left(-\frac{(2n+1)^2}{4\sigma/Le}\pi^2 t\right). \tag{23}$$

Once θ and φ are known, one can determine the function $f(t)$ in (19) by imposing the integral condition

$$\int_{-1}^{+1} v(x,t)\,dx = 0 \tag{24}$$

which states that the fluid volume is conserved. This condition is a consequence of the assumption that the fluid is Boussinesq-incompressible, see equation (9), and is therefore valid for all values of time and along any arbitrary horizontal cross-section. Integrating (19) with θ and φ given by (22) and (23), and invoking condition (24) gives $f(t) = 0$. Thus, the small-time solution to the velocity field is given by (19), (22) and (23) with $f = 0$. As mentioned earlier, the analytical solution presented in this section is used only as a tool for verifying the correctness of the numerical code which is developed for the fully numerical solution.

5. ANALYTICAL SOLUTION FOR THE STEADY STATE

5.1. *General case*

For the steady-state case, it is possible to find an analytical solution towards which the transient solution approaches asymptotically. Such a solution is valid for enclosures with relatively high aspect ratios, and in regions where end effects due to the presence of horizontal walls are negligible. In this subsection, the detailed procedure of deriving the analytical solution to the steady-state problem, valid for a rather large domain of parameter values, is outlined.

The numerical solution to the full problem indicates that after an initial and rather short period of time, during which a weak and stable stratification of the temperature and concentration fields is set up, the momentum, heat and mass transfer phenomena in the enclosure can be characterized by a slow evolution towards a steady state at which the temperature and concentration fields become linearly and stably stratified in the vertical direction. Moreover, for sufficiently high aspect ratios, and outside the end regions, the velocity vector proves to be predominantly vertical and independent of the vertical coordinate y. Guided by these observations, the proposed form of the steady-state analytical solution reads

$$\mathbf{u} = v(x)\bar{e}_y \tag{25}$$

$$\theta = -S_c y + \vartheta_c(x) \tag{26}$$

$$\varphi = S_T y + \vartheta_T(x) \tag{27}$$

where $S_c > 0$ and $S_T > 0$ are unknown constants and $v(x)$, $\vartheta_c(x)$ and $\vartheta_T(x)$ are unknown functions to be determined. One also needs an assumption for the pressure gradient term. Introducing (25)–(27) into equation (8) and rearranging the terms gives

$$v(x)\bar{e}_y = -\{\nabla P - R_c(S_c + NS_T)y\bar{e}_y\} - R_c\vartheta_c(x)\bar{e}_y + NR_c\vartheta_T(x)\bar{e}_y$$

which in turn renders the assumption

$$\nabla P = \{\Pi_y + R_c(S_c + NS_T)y\}\bar{e}_y \tag{28}$$

necessary for the pressure gradient. The quantity denoted by Π_y is an unknown constant which is determined later. The solution form assumed in (25)–(28) is a generalization, and application to double diffusive phenomena, of a model proposed by Prandtl [22] for mountain winds in stratified air. Trevisan and Bejan tried the aforementioned form of solution for double diffusive natural convection in both a Newtonian fluid [23] and a fluid-saturated porous medium [12]. However, in both cases, due to reasons discussed later, their solution proved to be valid only for the case of $Le = 1$ while, as the present analysis shows, it could in principle have been valid for any value of Le.

Substitution of (25)–(28) in (8)–(13), with $\partial/\partial t \equiv 0$, yields the equations

$$v(x) = -\Pi_y - R_c\vartheta_c(x) + R_cN\vartheta_T(x) \tag{29}$$

$$-v(x)S_c = \frac{\mathrm{d}^2\vartheta_c}{\mathrm{d}x^2} \tag{30}$$

$$v(x)S_T = Le\frac{\mathrm{d}^2\vartheta_T}{\mathrm{d}x^2} \tag{31}$$

and the boundary conditions

$$\frac{\mathrm{d}\vartheta_c}{\mathrm{d}x} = -1 \text{ at } x = \pm 1 \tag{32}$$

for the concentration profile, and, in the cooperating case,

$$\frac{\mathrm{d}\vartheta_T}{\mathrm{d}x} = +1 \text{ at } x = \pm 1 \tag{33}$$

for the temperature profile. By solving equations (29)–(31) subject to the boundary conditions (32) and (33), one can determine the unknown functions $v(x)$, $\vartheta_c(x)$ and $\vartheta_T(x)$ in terms of two integration constants and S_c, S_T and Π_y. In order to determine these five constants, five integral conditions have to be imposed on the solution. These conditions are briefly discussed below.

The velocity profile $v(x)$ should satisfy the condition of conservation of fluid volume (24), which is already mentioned in Section 4.

The total amount of solute has to be conserved, i.e.

$$\varepsilon\int_{-1}^{+1}\int_{-A}^{+A}\theta\,\mathrm{d}y\,\mathrm{d}x = \int_0^t\int_{-A}^{+A}\left\{\left(\frac{\partial\theta}{\partial x}\right)_{x=+1} - \left(\frac{\partial\theta}{\partial x}\right)_{x=-1}\right\}\mathrm{d}y\,\mathrm{d}t$$

which in view of (13) and (26) yields

$$\int_{-1}^{+1}\vartheta_c(x)\,\mathrm{d}x = 0. \tag{34}$$

Similarly, one can show that

$$\int_{-1}^{+1}\vartheta_T(x)\,\mathrm{d}x = 0. \tag{35}$$

In the problem studied here, since the prescribed gradients of temperature and concentration on both of the vertical walls are exactly the same, the integral conditions (24), (34) and (35) become equivalent to assuming that the functions $v(x)$, $\vartheta_c(x)$ and $\vartheta_T(x)$ are centrosymmetric.

For the steady-state case equation (10) can be rewritten as

$$\nabla\cdot(\mathbf{u}\theta - \nabla\theta) = 0$$

which in turn, after integrating throughout the control volume V shown in Fig. 1(b), applying Gauss' theorem and invoking the boundary conditions (12) and (13), can be reduced to

$$\int_{-1}^{+1}(\mathbf{u}\theta - \nabla\theta)\cdot\bar{e}_y\,\mathrm{d}x = 0. \tag{36}$$

The physical interpretation of the integral condition (36) is that, at steady state, the net diffusive and convective transports of solute through any horizontal cross-section of the cavity balance each other exactly, see refs. [3, 6]. Inserting (25) and (26) into (36), and invoking (24), gives

$$\int_{-1}^{+1}v\vartheta_c\,\mathrm{d}x + 2S_c = 0. \tag{37}$$

Similarly, one can show that

$$\int_{-1}^{+1} v\vartheta_T \,\mathrm{d}x - 2LeS_T = 0. \tag{38}$$

The physical interpretation of (38) is that, at steady state, the net diffusive and convective transports of enthalpy through any horizontal cross-section of the cavity are in exact balance, see ref. [3].

The value of the constant Π_y can be readily determined by integrating the expression (29) across a horizontal cross-section, which, in view of the integral conditions (24), (34) and (35), gives $\Pi_y = 0$.

The linear system of second-order coupled differential equations (29)–(31), subject to the boundary conditions (32) and (33) and the integral conditions (24), (34), (35), (37) and (38) define a simple mathematical problem that can be solved easily. It proves expedient to introduce the notations $\Omega = \sqrt{(R_c S_c + R_T S_T)}$ and $B = (NR_c S_c - R_T S_T)/(R_c S_c + R_T S_T)$, where $R_T = R_c(N/Le)$ is the thermal Rayleigh–Darcy number. In terms of the yet unknown constants Ω, B, S_c and S_T, the exact solution to the problem then reads

$$v(x) = \frac{\Omega(1+B)}{S_c \cosh(\Omega)} \sinh(\Omega x) \tag{39}$$

$$\vartheta_c(x) = -\frac{1+B}{\Omega \cosh(\Omega)} \sinh(\Omega x) + Bx \tag{40}$$

$$\vartheta_T(x) = -\frac{S_T}{LeS_c}\vartheta_c(x) + \left(1 - \frac{S_T}{LeS_c}\right)x. \tag{41}$$

The integral conditions (24), (34) and (35) have been employed in deriving the solution given by (39)–(41). The linear terms in (40) and (41), which are due to the different values of solutal and thermal diffusivities ($Le \neq 1$), see Subsection 5.2.2, are of utmost importance in the present analysis. It is indeed possible to motivate the presence of these linear terms by purely physical arguments. To begin with, consider the case of isothermal buoyancy-driven convection due to prescribed gradients of concentration, see Fig. 2. The velocity and concentration profiles in such a case adjust themselves to the needs of solute flux dictated by these gradients. Now, suppose that a temperature gradient is also imposed on the side-walls. If the prescribed temperature and concentration gradients augment each other, the amplitude of fluid velocity will increase at each point due to the increase of the buoyancy forces that drive the whole motion, Fig. 2(a). As a result, the convective transport of solute will be enhanced, see Fig. 2(b). Compared to the isothermal case, a larger amount of solute will thus be removed from the high-concentration wall ($x = -1$) and supplied to the low-concentration wall ($x = +1$). Since the mass flux conditions at these walls are unaltered, the thermally enhanced convective transport of solute builds up a solute surplus region near the low-concentration wall and a corresponding solute deficit region near the high-concentration wall. This in turn leads to a backward diffusion of solute from the surplus to the deficit region, hence giving rise to a horizontal gradient of concentration in the bulk fluid. The appearance of horizontal temperature gradients in the bulk fluid also can be motivated by similar arguments.

Now it remains to determine the values of S_c and S_T. Introducing the expressions (39)–(41) into the integral conditions (37) and (38), leads to the nonlinear and coupled system of algebraic equations

$$S_c^2 - \frac{(1+B)^2}{1+\cosh(2\Omega)}\left(\frac{\sinh(2\Omega)}{2\Omega} - 1\right) + B(1+B)\left(1 - \frac{\tanh(\Omega)}{\Omega}\right) = 0 \tag{42}$$

$$\left(1 - \frac{1}{Le^2}\right)S_T - \left(1 - \frac{1}{Le}\frac{S_T}{S_c}\right)\left(1 - \frac{\tanh(\Omega)}{\Omega}\right)\frac{1+B}{LeS_c} = 0 \tag{43}$$

from which S_c and S_T can be determined for given values of R_c, Le and N. Obviously, for the general case, the equation system defined by (42) and (43) has to be solved by numerical methods, e.g. by Newton–Raphson's method. However, this is by far a much easier task than numerically solving the full set of the nonlinear and coupled partial differential equations that are used to model momentum, mass and heat conservation in this problem. For the two extreme cases of boundary layer type solute-driven and heat-driven natural convection, it is possible to derive approximate solutions to (42) and (43). These solutions are given in Subsections 5.2.3 and 5.2.4 and then supported by pure scale analysis arguments in Section 6.

Once the solution is fully determined, one can compute the overall Sherwood (Sh) and Nusselt (Nu) numbers, which are usually of interest in engineering applications. In terms of the already known parameters Le, S_c, S_T, B and Ω, one can show that

$$Sh = \frac{2A}{\frac{1}{2}\int_{-A}^{+A}\{(\theta)_{x=-1} - (\theta)_{x=+1}\}\,\mathrm{d}y} \approx \frac{2}{\vartheta_c(-1) - \vartheta_c(+1)} = \frac{1}{\frac{1+B}{\Omega}\tanh(\Omega) - B} \tag{44}$$

and

$$Nu = \frac{2A}{\frac{1}{2}\int_{-A}^{+A}\{(\varphi)_{x=+1} - (\varphi)_{x=-1}\}\,\mathrm{d}y} \approx \frac{2}{\vartheta_T(+1) - \vartheta_T(-1)} = \left[\frac{S_T}{LeS_c}\frac{1}{Sh} + 1 - \frac{S_T}{LeS_c}\right]^{-1} \tag{45}$$

from which Sh and Nu can be determined. The first and the last expressions on the right-hand sides of (44) and (45) are used for evaluating the fully numerical

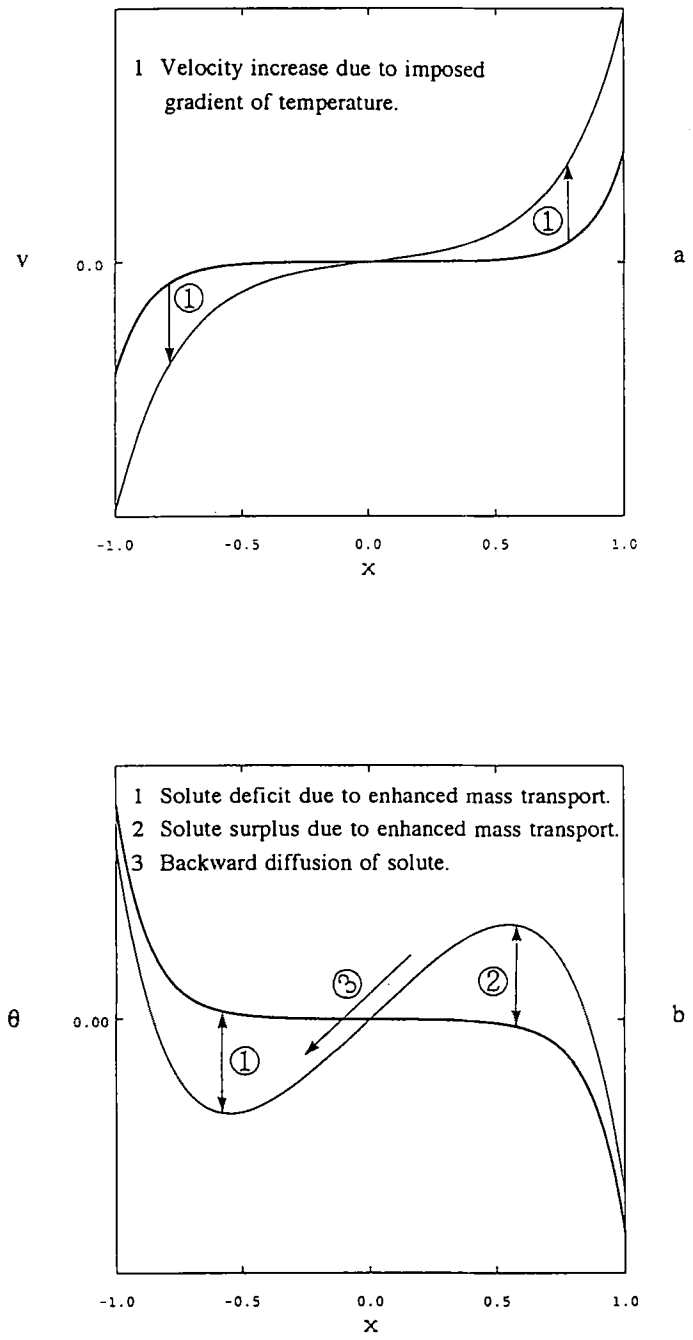

FIG. 2. Tentative profiles of concentration and velocity before (thick line) and after (thin line) imposing a cooperative temperature gradient. (a) Velocity profiles, (b) concentration profiles.

and the analytical solutions, respectively. Note that according to (44) and (45) the analytical expressions for *Sh* and *Nu* do not depend on the height of the enclosure. This can be attributed to the fact that in the domain of validity of the analytical solution, i.e. for slender enclosures, the wall to wall concentration and temperature differences at any arbitrary horizontal cross-section are independent of the vertical position of the cross-section.

5.2. *Special cases*

In deriving the analytical solution, given by (25)–(27) and (39)–(43), no restrictions are imposed on the values of Le, R_c and N, and therefore the solution is, in principle, valid for any values of these input parameters. This is of course true as long as the aspect ratio of the cell is high enough for the end effects to be confined to small regions near the top and the bottom of the enclosure. In the next subsections, the

interesting and often encountered case of boundary layer solution will be discussed in some detail. Thereafter, in Subsection 5.2.2, the case of $Le = 1$ will be treated in order to shed some light on the discrepancy between the present analysis and that by Trevisan and Bejan [12]. Subsections 5.2.3 and 5.2.4 are concerned with two extreme cases, namely solute-driven and heat-driven boundary layer type flows.

5.2.1. *Boundary layer approximation.* It is possible to further simplify the analytical solution by assuming that $e^{2\Omega} \gg 1$ ($\Omega > 3$). This occurs when, e.g., $R_c \gg 1$, and from a physical point of view, it means that the velocity and concentration fields have boundary layer character. Whether or not the temperature field too has boundary layer character depends on the values of N and Le. Invoking the aforementioned simplifying assumption, the analytical solution presented in the foregoing section can be reduced to

$$v(x) = \mp \frac{\Omega(1+B)}{S_c} e^{-\Omega(1\pm x)} \tag{46}$$

$$\vartheta_c(x) = \pm \frac{1+B}{\Omega} e^{-\Omega(1\pm x)} + Bx. \tag{47}$$

The upper and lower signs are valid in the $x \sim -1$ and $x \sim +1$ boundary layers, respectively. The expressions (46) and (47) show that the inverse of the parameter Ω can be interpreted as a measure of the thickness of the vertical buoyancy layers attached to the vertical side-walls. Moreover, they show that the hydrodynamic and concentration boundary layer thicknesses are equal. This can be attributed to the stable density stratification of the bulk fluid, which hampers the motion there and compels the hydrodynamic boundary layer to retreat towards the vertical walls and thus to confine itself to regions of high horizontal gradients of density. In cases where the temperature field too has boundary layer character, its thickness will, according to (41), be equal to that of the hydrodynamic and concentration boundary layers. This occurs irrespective of how large or small Le is.

It is instructive to rewrite equation (47) as

$$\vartheta_c \equiv \Theta(x, \xi) = \pm \frac{1+B}{\Omega} e^{-\xi} + Bx \tag{48}$$

in which ξ is the boundary layer coordinate defined by $\xi = \Omega(1 \pm x)$. Expression (48) shows that when ξ becomes large, i.e. on approaching the outer limit of the boundary layer, the function denoted by Θ, and thereby even ϑ_c, becomes a straight line. In the formal language of mathematics, this is equivalent to the relationship

$$\lim_{\xi\to\infty} [\vartheta_c] \approx Bx. \tag{49}$$

Similarly, one can show that

$$\lim_{\xi\to\infty} [\vartheta_T] \approx \left[1 - \frac{(1+N)R_cS_T}{Le(R_cS_c + R_TS_T)}\right] x. \tag{50}$$

In ref. [12], the authors assumed from the very beginning that $v(x)$, $\vartheta_c(x)$ and $\vartheta_T(x)$ were boundary layer functions and they chose to seek a solution that fulfilled the core condition

$$\lim_{\xi\to\infty} [\vartheta_c, \vartheta_T] = 0.$$

In the course of their analysis, they concluded that their solution was valid for the case of $Le = 1$ only. This conclusion is in full agreement with the results of the present analysis which show that the right-hand sides of (49) and (50) become identically equal to zero if and only if $Le = 1$.

5.2.2. *The case of* $Le = 1$. Assuming that the thermal and solutal diffusivities are exactly equal, i.e. $Le = 1$, equation (43) reduces to the simple form of $S_T = S_c$. This in turn gives $B = 0$ and $(1+N)R_cS_T = Le(R_cS_c + R_TS_T)$, thus making the right-hand sides of (49) and (50) equal to zero. The solution to the problem is then given by

$$\vartheta_c = -\vartheta_T = -\frac{S_c}{\Omega^2} v = -\frac{1}{\Omega \cosh(\Omega)} \sinh(\Omega x),$$

where $\Omega = \sqrt{(R_cS_c(1+N))}$. S_c should be computed from the reduced form of equation (42) which reads

$$S_c^2 - \frac{1}{1+\cosh(2\Omega)} \left(\frac{\sinh(2\Omega)}{2\Omega} - 1\right) = 0.$$

Once the value of S_c, and thereby Ω, is known, the Sherwood and Nusselt numbers can be calculated from

$$Sh = Nu = \frac{\Omega}{\tanh(\Omega)}$$

which is the reduced version of (44) and (45).

If one further assumes that the solution has boundary layer character, i.e. if $\Omega > 3$, the above equations lead to the following solution

$$\vartheta_c = -\vartheta_T = -\frac{S_c}{\Omega^2} v = \pm \frac{1}{\Omega} e^{-\Omega(1\pm x)},$$

where $\Omega = 2^{-1/5}(1+N)^{2/5} R_c^{2/5}$,

$$S_c = S_T = 2^{-2/5}(1+N)^{-1/5} R_c^{-1/5}$$

and

$$Sh = Nu = 2^{-1/5}(1+N)^{2/5} R_c^{2/5},$$

which agrees with the results by Trevisan and Bejan [12].

Before closing this subsection, the following comments may be in order.

(i) From a practical point of view, the case of $Le = 1$ has a very limited value since, at least to the knowledge of the present author, it is not possible to find a solute with exactly the same diffusivity as heat.

(ii) The case of $Le = 1$ does not belong to the class of problems that are described as 'double diffusive phenomena'.

(iii) From a mathematical point of view, the treat-

ment of the $Le = 1$ case can, for the steady state (or, if $\sigma = \varepsilon$, even for the transient case), be substantially simplified by introducing an auxiliary function Φ defined by $\Phi = (\theta - N\varphi)/(1+N)$. The equation system (8)–(14) can then be reformulated as

$$\mathbf{u} = -\nabla P - R_c(1+N)\Phi \bar{e}_y,$$

$$\nabla \cdot \mathbf{u} = 0, \quad \sigma \frac{\partial \Phi}{\partial t} + \mathbf{u} \cdot \nabla \Phi = \nabla^2 \Phi$$

$$\frac{\partial \Phi}{\partial y} = 0 \text{ and } v = 0 \text{ at } |y| = A,$$

$$\frac{\partial \Phi}{\partial x} = -1 \text{ and } u = 0 \text{ at } |x| = 1$$

$$\Phi = 0 \text{ and } \mathbf{u} = 0 \text{ at } t = 0.$$

This modified version of the problem represents buoyancy-driven natural convection due to the gradients of one single property, i.e. Φ. Numerical and analytical investigations of this problem are already available in the literature, see e.g. refs. [3] and [6].

As a concluding remark, it should be emphasized that the linear terms in (40) and (41) are the outcome of the double diffusive feature of the present study and excluding them from this analysis would seriously restrict the applicability and usefulness of the analytical solution reported in this paper.

5.2.3. *Solute-driven boundary layer approximate solution.* Under the assumptions that $N \ll 1$, $R_c \gg 1$ and R_T small, which imply that the flow is solute-driven boundary layer type, one can derive an approximate solution to equations (42) and (43). Omitting the algebric details of the derivation, the approximate values of S_c and S_T read

$$S_c = 2^{-2/5} R_c^{-1/5}$$

and

$$S_T = 2^{2/5} Le^{-1} R_c^{1/5}(1 - 2^{4/5} Le^{-2} R_c^{2/5}),$$

and thus the corresponding approximate values of the Sherwood and Nusselt numbers become

$$Sh = 2^{-1/5} R_c^{2/5}$$

and

$$Nu = 1 + 2^{4/5} Le^{-2} R_c^{2/5}(1 - 2^{1/5} R_c^{-2/5})(1 - 2^{4/5} Le^{-2} R_c^{2/5}).$$

The correction terms in the expressions for S_T and Nu apply if $R_c \ll 0.25 Le^5$. In view of the usually large value of Le, this condition is not inconveniently restrictive.

Another interesting quantity here is the order of magnitude of the thickness of the hydrodynamic and concentration (vertical) boundary layers, which in view of the approximations of this subsection becomes

$$\delta \sim \frac{1}{\Omega} = 2^{1/5} R_c^{-2/5}.$$

The temperature profile in this case is not of the boundary layer type.

The approximate solution presented in this subsection is in good agreement with the fully numerical calculations. This solution is, to the hightest order of magnitude, reconfirmed in Subsection 6.1 on scaling grounds.

5.2.4. *Heat-driven boundary layer approximate solution.* In this subsection it is assumed that fluid flow is mainly due to the gradients of temperature, i.e. $N \gg 1$, $R_T \gg 1$ and R_c small. Under these circumstances, the approximate solution to equations (42) and (43) becomes

$$S_c = 2^{-2/5} Le^{-1} R_T^{1/5} \quad \text{and} \quad S_T = 2^{-2/5} R_T^{-1/5},$$

yielding the following approximate values for the Sherwood and Nusselt numbers

$$Sh = 2^{4/5} R_T^{2/5} \quad \text{and} \quad Nu = 2^{-1/5} R_T^{2/5}.$$

For the sake of brevity, algebraic details are omitted. Note that the Sherwood number depends on the thermal Rayleigh–Darcy number only. This does not agree with the similarity solution results by Trevisan and Bejan [12], according to which, in the heat-driven limit and for $Le \gg 1$

$$Sh = 1.007952 \sqrt{\frac{Le}{A}} R_T^{3/10}$$

provided that $4R_T > 1$.

The thickness of the hydrodynamic, concentration and temperature (vertical) boundary layers can then be estimated by

$$\delta \sim \frac{1}{\Omega} = 2^{1/5} R_T^{-2/5}.$$

The approximate solution given in this subsection, as in the previous one, agrees well with the fully numerical solution. In order to remove any doubts about the correctness of these results, they are reconfirmed in Subsection 6.2 by resorting to pure scale analysis.

6. SCALE ANALYSIS

In the general case, the contribution to the buoyancy forces of neither the gradients of temperature nor those of concentration can be neglected. Under such circumstances, the quantities of interest involved in the problem are related in so complicated a way that would not allow estimations of their orders of magnitudes by scale analysis. However, at steady state, for the two limiting cases of solute-driven and heat-driven boundary layer type natural convection, order of magnitude estimates can be derived on scaling grounds. This section is meant to confirm the approximate solutions of Subsections 5.2.3 and 5.2.4 by scale analysis arguments and thus lend further support to both the numerical and analytical solutions that are presented in this paper. Throughout this section, it is

assumed that $A \gg 1$, $Le > 1$ and that at least the velocity and the concentration fields have boundary layer character. It is moreover assumed that the concentration and temperature fields are stably stratified in the vertical direction. The notations $\mathscr{V}$, $\mathscr{d}$ and $\mathscr{L}$ (Fig. 1(b)) are used to denote the scales of vertical velocity, vertical boundary layer thickness and vertical length scales, respectively.

6.1. *Solute-driven boundary layer type natural convection*

Suppose that the buoyancy forces that drive the fluid motion in the enclosure are mainly due to the gradients of solute concentration, i.e. $N \ll 1$. The concentration variation over the thickness of the vertical boundary layers is then typically $\Lambda^{(c)}\mathscr{d}$. In view of the solutal stratification of the fluid, it is reasonable to assume that, in the vertical direction, the aforementioned variation of concentration takes place over an unknown vertical distance $\mathscr{L}_c$. The balance equations to be satisfied by the three unknown scales $\mathscr{V}$, $\mathscr{d}$ and $\mathscr{L}_c$ are as follows

momentum balance:

$$\frac{\mu}{k}\mathscr{V} \sim \rho g \beta \Lambda^{(c)} \mathscr{d}$$

local balance of solute transport:

$$\mathscr{V}\frac{\Lambda^{(c)}\mathscr{d}}{\mathscr{L}_c} \sim D\frac{\Lambda^{(c)}\mathscr{d}}{\mathscr{d}^2}$$

global balance of solute transport:

$$2\mathscr{d}\mathscr{V}\Lambda^{(c)}\mathscr{d} \sim 2hD\frac{\Lambda^{(c)}\mathscr{d}}{\mathscr{L}_c}.$$

The last equation, which originates from the dimensional version of the integral condition (36), states that the vertical convective and diffusive net transports of solute should be comparable. Solving the balance equations for $\mathscr{V}$, $\mathscr{d}$ and $\mathscr{L}_c$ one obtains

$$\mathscr{d} \sim hR_c^{-2/5}, \quad \mathscr{V} \sim \frac{D}{h}R_c^{3/5} \quad \text{and} \quad \mathscr{L}_c \sim hR_c^{-1/5}.$$

The order of magnitude of the vertical gradient of concentration can now be deduced according to

$$\frac{\partial c}{\partial y} \sim \frac{\Lambda^{(c)}\mathscr{d}}{\mathscr{L}_c} \sim \Lambda^{(c)}R_c^{-1/5}.$$

The temperature field in this case is advected by the flow field that the concentration gradients generate. The scale of temperature variations in the horizontal direction is assumed to be $\Lambda^{(T)}h$, which is a conductive scale implying that the horizontal profile of temperature is not of boundary layer type. In the vertical direction, a temperature variation of order $\Lambda^{(T)}h$ occurs over a vertical length scale $\mathscr{L}_T$. $\mathscr{L}_T$ can be obtained from the balance equation

global balance of heat transport:

$$2\mathscr{d}\mathscr{V}\Lambda^{(T)}h \sim 2h\kappa\frac{\Lambda^{(T)}h}{\mathscr{L}_T},$$

which gives

$$\mathscr{L}_T \sim hLeR_c^{-1/5}.$$

The order of magnitude of the vertical temperature gradient can now be estimated by

$$\frac{\partial T}{\partial y} \sim \frac{\Lambda^{(T)}h}{\mathscr{L}_T} \sim \Lambda^{(T)}Le^{-1}R_c^{1/5}.$$

The equation for the local balance of thermal energy in this case merely translates into the condition $Le\,R_c^{-2/5} > 1$ that should be fulfilled to render the assumption $\Delta T \sim \Lambda^{(T)}h$ valid.

As can be seen, the quantities $\mathscr{d}$, $\partial c/\partial y$ and $\partial T/\partial y$ derived here, are in good agreement with their non-dimensional counterparts δ, S_c and S_T, in Subsection 5.2.3.

6.2. *Heat-driven boundary layer type natural convection*

In this subsection, the buoyancy forces are assumed to be mainly due to the gradients of temperature. A typical variation of temperature $\Lambda^{(T)}\mathscr{d}$ occurs here over a horizontal length scale $\mathscr{d}$ or a vertical length scale $\mathscr{L}_T$. The balance equations for the temperature related unknown scales are

momentum balance:

$$\frac{\mu}{k}\mathscr{V} \sim \rho g \alpha \Lambda^{(T)} \mathscr{d}$$

local balance of heat transport:

$$\mathscr{V}\frac{\Lambda^{(T)}\mathscr{d}}{\mathscr{L}_T} \sim \kappa\frac{\Lambda^{(T)}\mathscr{d}}{\mathscr{d}^2}$$

global balance of heat transport:

$$2\mathscr{d}\mathscr{V}\Lambda^{(T)}\mathscr{d} \sim 2h\kappa\frac{\Lambda^{(T)}\mathscr{d}}{\mathscr{L}_T},$$

from which one obtains

$$\mathscr{d} \sim hR_T^{2/5}, \quad \mathscr{V} \sim \frac{\kappa}{h}R_T^{3/5} \quad \text{and} \quad \mathscr{L}_T \sim hR_T^{-1/5}.$$

The order of magnitude of the vertical gradient of temperature then becomes

$$\frac{\partial T}{\partial y} \sim \frac{\Lambda^{(T)}\mathscr{d}}{\mathscr{L}_T} \sim \Lambda^{(T)}R_T^{-1/5}.$$

The scale analysis for the concentration field, which is being advected by the velocity field due to the thermal buoyancy forces, proves to be a matter of some complexity since it can offer different possibilities with different results. At this stage, two additional balance equations can be set up, one for the local and one for the global balance of solute transport. This means that one can estimate the orders of two unknown scales. It is also possible to use one of these equations to derive the expression for one unknown scale and

the remaining equation to derive a validity condition. In the previous subsection, e.g., it was assumed that a conductive temperature scale $\Lambda^{(T)}h$, prevailed in both the vertical and horizontal directions and that the only temperature related unknown scale was the vertical length scale $\mathscr{L}_T$. The global balance of heat transport provided the latter while the local balance was interpreted as a validity condition. A similar choice cannot be made in the present case since the horizontal profile of concentration in the heat-driven case, unlike its thermal counterpart in the solute-driven one, is not diffusive. This fact is clearly illustrated by both the fully numerical and the analytical solutions. In order to go further from here, it is necessary to assume something about the kind of solution one is seeking to verify through order-of-magnitude scaling analysis. According to the fully numerical results, given in Section 7, depending on the aspect ratio A of the enclosure, two different patterns of solution can be observed for the concentration field: (i) the bulk fluid is rather homogeneous and the vertical boundary layers of concentration are thinner than those of the velocity and temperature fields, and (ii) the concentration field is stably stratified in the vertical direction and its vertical boundary layers are as thick as their thermal and hydrodynamic counterparts. The latter pattern occurs for $A \gg 1$ and will be the focus of attention during the rest of this subsection. It is reasonable, and indeed proves to be the only appropriate alternative, to recognize the two unknown quantities Δc_v and $\mathscr{L}_c$, which represent the vertical concentration and length scales, respectively, as the scales that remain to be resolved. The variation of concentration across the vertical boundary layer is of order $\Lambda^{(c)}\mathscr{d}$. The balance equations for Δc_v and $\mathscr{L}_c$ read

local balance of solute transport:

$$\mathscr{V}\frac{\Delta c_v}{\mathscr{L}_c} \sim D\frac{\Lambda^{(c)}\mathscr{d}}{\mathscr{d}^2}$$

global balance of solute transport:

$$2\mathscr{d}\mathscr{V}\Delta c_v \sim 2hD\frac{\Delta c_v}{\mathscr{L}_c},$$

which in turn yield

$$\Delta c_v \sim \Lambda^{(c)}hLe^{-2}R_T^{-2/5} \quad \text{and} \quad \mathscr{L}_c \sim hLe^{-1}R_T^{-1/5}.$$

The order of magnitude of the vertical gradient of concentration becomes

$$\frac{\partial c}{\partial y} \sim \frac{\Delta c_v}{\mathscr{L}_c} \sim \Lambda^{(c)}Le^{-1}R_T^{-1/5}.$$

The quantities $\mathscr{d}$, $\partial c/\partial y$ and $\partial T/\partial y$ derived here compare well with δ, S_c and S_T, given in Subsection 5.2.4.

7. RESULTS AND DISCUSSIONS

A large number of fully numerical computations has been carried out to investigate the transient and the steady-state behaviours of the problem considered here. Comparisons are made between numerical and analytical solutions for small values of time, in order

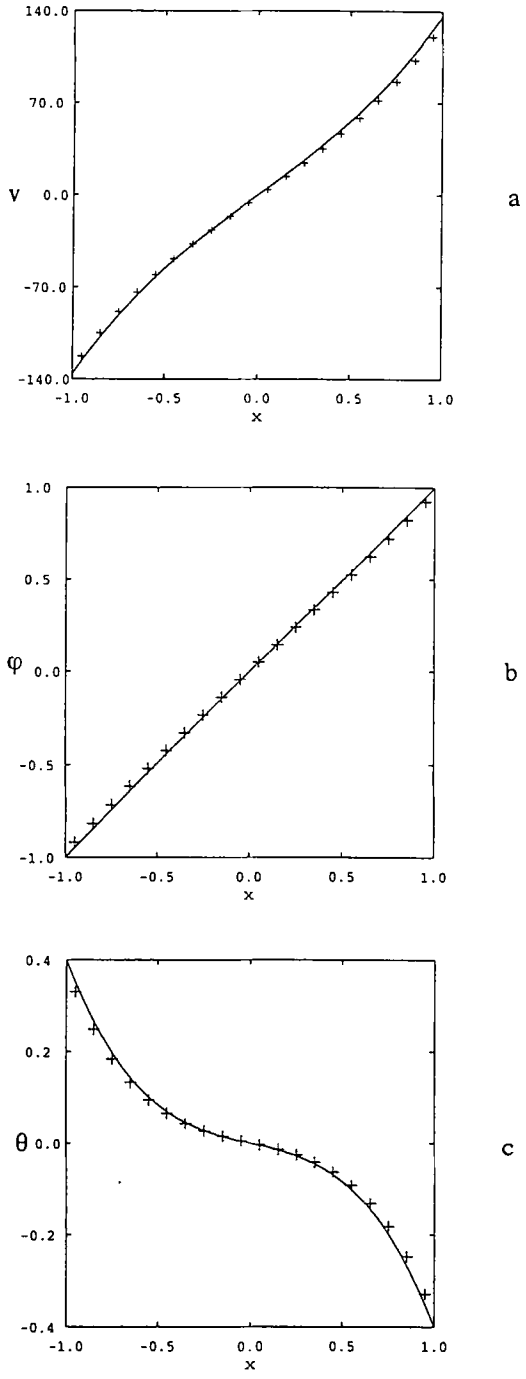

FIG. 3. Comparison between fully numerical (+) and analytical (——) solutions for small t, $\sigma = \varepsilon = 0.8$, $R_c = 100$, $Le = 10$, $N = 1$, $y = 0$ and $t = 0.1$. (a) Velocity profile, (b) temperature profile and (c) concentration profile.

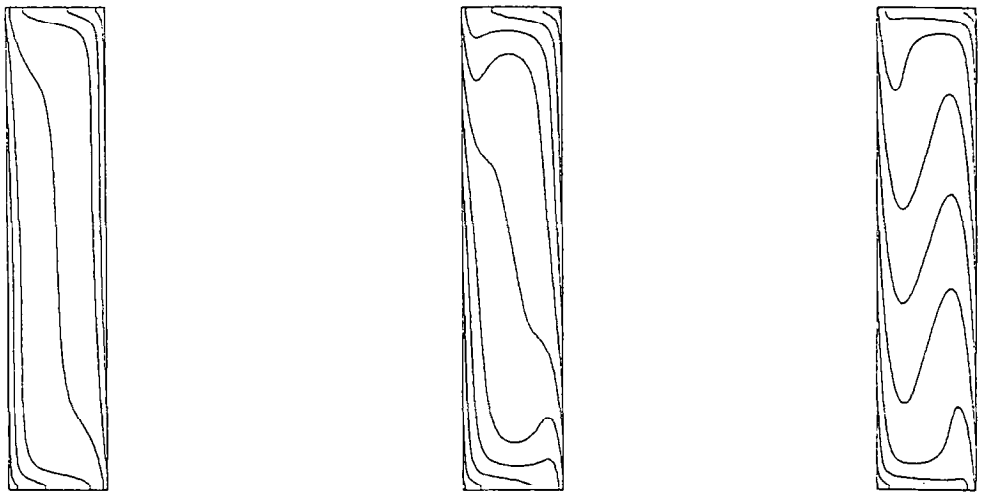

FIG. 4. Evolution of the concentration field for $A = 5$, $R_c = 250$, $Le = 25$ and $N = 0.5$. (a) $t = 0.05$, $-0.4 \leqslant \theta \leqslant 0.4$ and $\Delta\theta = 0.1$; (b) $t = 0.1$, $-0.5 \leqslant \theta \leqslant 0.5$ and $\Delta\theta = 0.1$; and (c) $t = 5$, $-0.5 \leqslant \theta \leqslant 0.5$ and $\Delta\theta = 0.1$. θ decreases from the lower left corner to the upper right corner.

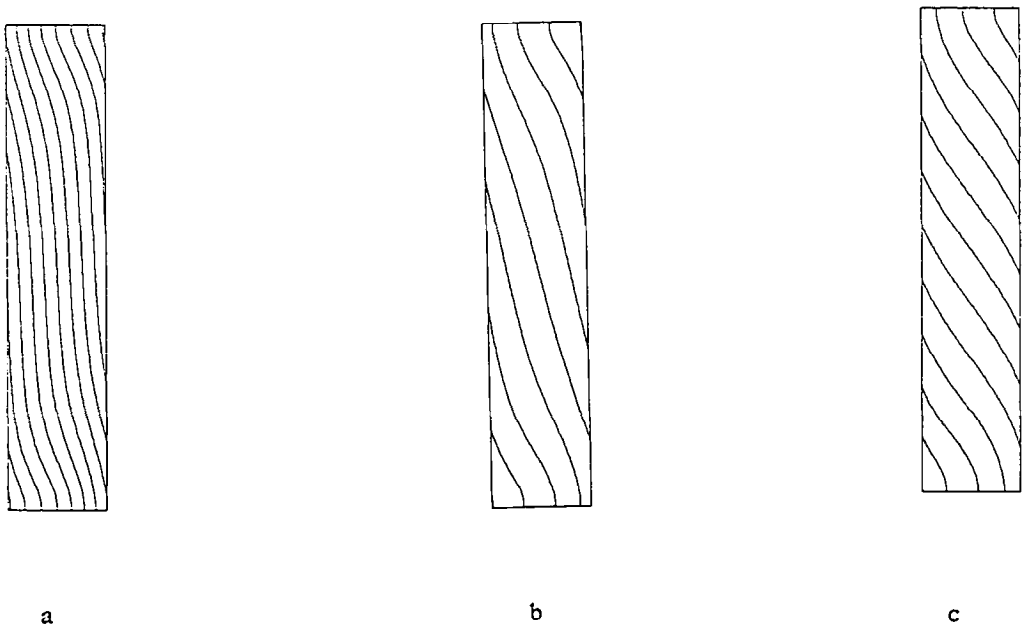

FIG. 5. Evolution of the temperature field for $A = 5$, $R_c = 250$, $Le = 25$ and $N = 0.5$. (a) $t = 0.05$, $-1.5 \leqslant \varphi \leqslant 1.5$ and $\Delta\varphi = 0.25$; (b) $t = 0.1$, $-2 \leqslant \varphi \leqslant 2$ and $\Delta\varphi = 0.5$; and (c) $t = 5$, $-2.5 \leqslant \varphi \leqslant 2.5$ and $\Delta\varphi = 0.5$. φ increases from the lower left corner to the upper right corner.

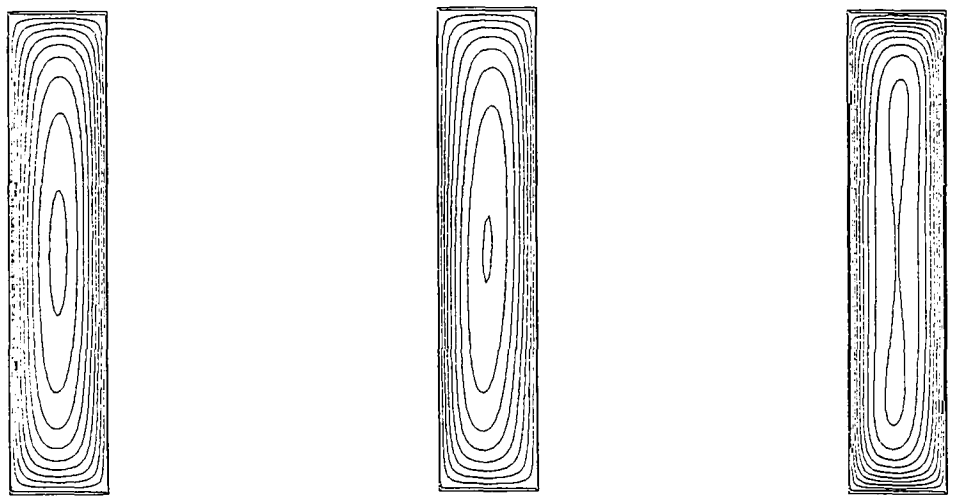

FIG. 6. Evolution of the streamlines for $A = 5$, $R_c = 250$, $Le = 25$ and $N = 0.5$. (a) $t = 0.05$, $-45 \leqslant \psi \leqslant 0$ and $\Delta\psi = 5$; (b) $t = 0.1$, $-40 \leqslant \psi \leqslant 0$ and $\Delta\psi = 5$; and (c) $t = 5$, $-22.5 \leqslant \psi \leqslant 0$ and $\Delta\psi = 2.5$. ψ decreases inwards from the boundaries.

to validate the numerical code, and for steady state, in order to verify the steady-state analytical solution. The results are plotted as contour lines and profiles of the computed quantities of interest. With a view to illustrate the crucial features and the domain of the validity of the steady-state analytical solution, a representative selection of the results is chosen and presented in Figs. 3–16.

The numerically determined profiles of velocity, temperature and concentration for small values of time are compared with their analytical counterparts in Figs. 3(a)–(c). For the case shown in these Figures, the agreement between the two solutions is good for $t < 0.1$ and satisfactory for $t = 0.1$ while it gradually deteriorates for $t > 0.1$. This is due to the fact that, as time passes, the appearance of vertical gradients renders a solution of the form given in (18) invalid. The analytical solution is valid for values of t that are smaller than the time interval needed for a fluid particle to travel from the top to the bottom of the enclosure, i.e. for $t \leqslant \tau$, where $\tau \sim 2A/R_c(1+N)$ according to (19), (22) and (23).

The transient evolution of the concentration, temperature and velocity fields is illustrated in Figs. 4–6. Figures 4(a)–6(a) show that for small values of time, the transport phenomena are largely one dimensional and dominated by horizontal diffusion. Moreover, the end effects are shown to be confined to fairly small regions at the top and the bottom of the cell. Figures 4(b)–6(b) show that after some time, vertical gradients of concentration and temperature appear in the fluid. Thus, the aforementioned fields, and thereby the density field, tend towards a stable vertical stratification. This in turn is followed by a reduction in the magnitude of velocity throughout the fluid. The rest of the process can be characterized by a slow approach towards the steady state at which the concentration and temperature fields are stably and linearly stratified in the vertical direction, see Figs. 4(c)–6(c). These observations form the grounds on which the development of the analytical solution is based. As will be discussed later, this pattern of solution is observed if the aspect ratio is not small. The contour lines of concentration and temperature in Figs. 4(c) and 5(c), unlike their isosolutal and isothermal counterparts in refs. [3] and [6], are not horizontal in the core region. This phenomenon is special for double diffusive natural convection and can be attributed to the difference in thermal and solutal diffusivities.

The comparison between numerical and analytical solutions at steady state is shown in Figs. 7–10. The vertical profiles of concentration and temperature at $x = 0$ are given in Figs. 7(a) and (b). These Figures lend support to the assumption that at steady state, and for sufficiently high aspect ratios, the end effects are restricted to small regions around the top and bottom walls of the enclosure and that the core region is linearly stratified. These assumptions are used in the development of the analytical solution in Section 5. One can also conclude from Figs. 7(a) and (b) that, for $Le > 1$, the horizontal layers at the top and bottom of the enclosure are *thinner* for the temperature field than for the concentration field. Extensive numerical calculations show that this conclusion applies regard-

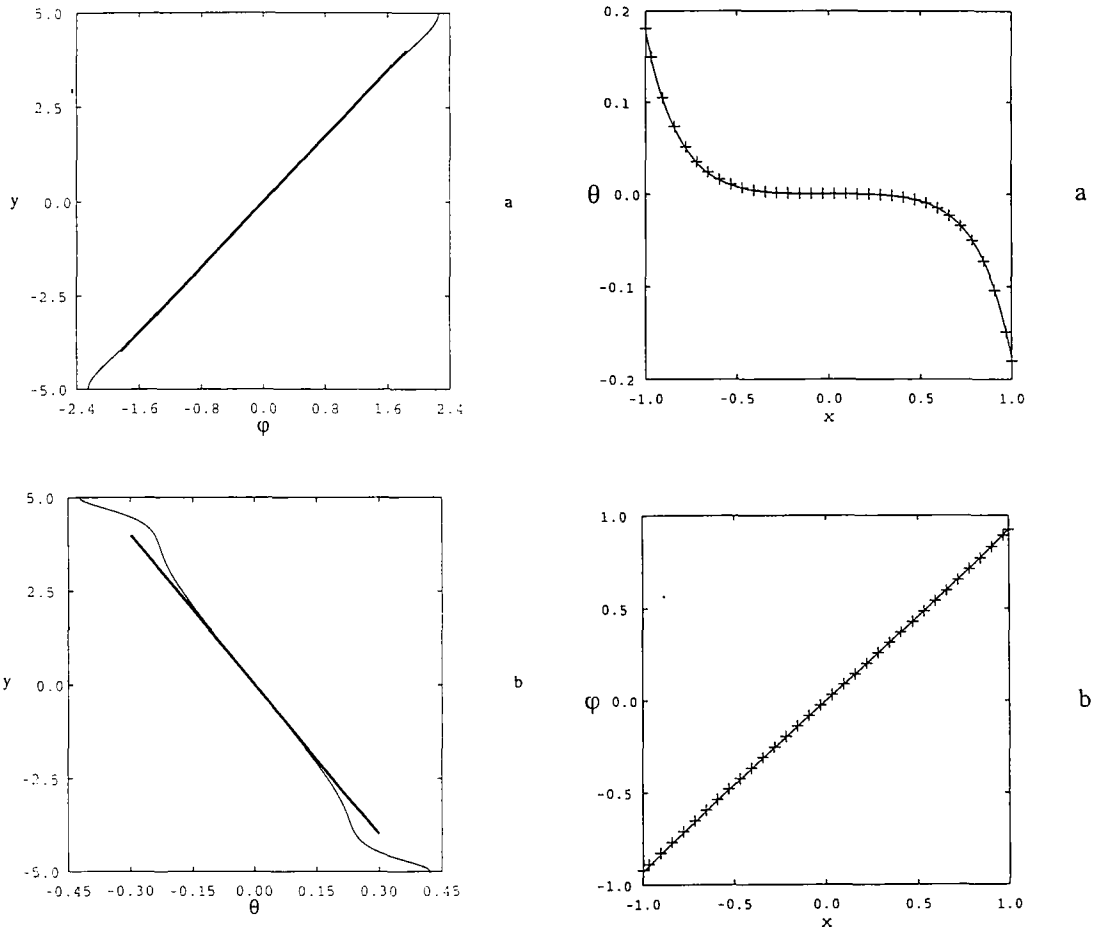

FIG. 7. Comparison between fully numerical (thin line) and analytical (thick line) solutions at steady state for $A = 5$, $R_c = 100$, $Le = 10$, $N = 1$, $x = 0$. (a) Temperature, and (b) concentration.

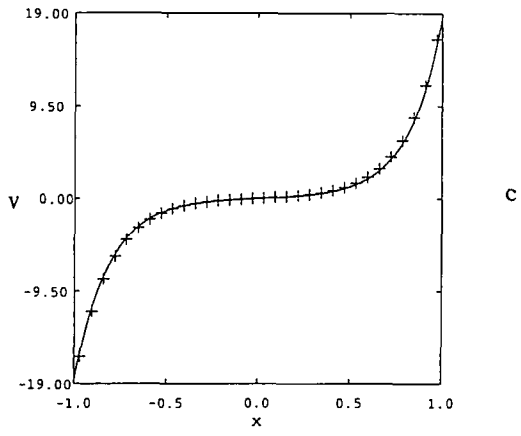

FIG. 8. Comparison between fully numerical (+) and analytical (——) solutions at steady state for $A = 10$, $R_c = 100$, $Le = 10$, $N = 0.01$ (solute-driven natural convection), $y = 0$. (a) Concentration, (b) temperature, and (c) velocity.

less of whether the flow is solute-driven, solute- and heat-driven or heat-driven.

In Figs. 8–10, numerical and analytical profiles of concentration, temperature and velocity at $y = 0$ are compared. The agreement between the two is shown to be good. In Fig. 8, fluid flow is mainly due to concentration variations, i.e. $v \sim R_c\theta$, compare Figs. 8(a) and (c). In Fig. 9, fluid flow is due to the combined effects of concentration and temperature variations. Finally, in Fig. 10, fluid flow is mainly due to temperature variations, i.e. $v \sim R_c N\varphi$, compare Figs. 10(b) and (c). The following rather interesting phenomena can be observed in these Figures:

(i) If the flow is driven by solute concentration gradients (the component with low diffusivity), the horizontal profile of temperature (the component with high diffusivity) becomes a conductive profile without a boundary layer character, see Fig. 8(b). In the opposite case, i.e. when the component with high diffusivity drives the motion, the horizontal profile of the component with low diffusivity will have a boundary layer form, see Fig. 10(a).

(ii) The profiles with boundary layer character have the same boundary layer thicknesses, see e.g. Figs. 8(a) and (c) or 10(a)–(c). (The solution in Fig. 9 has a weak boundary layer character.) This occurs despite the rather large value of the Lewis number. Moreover,

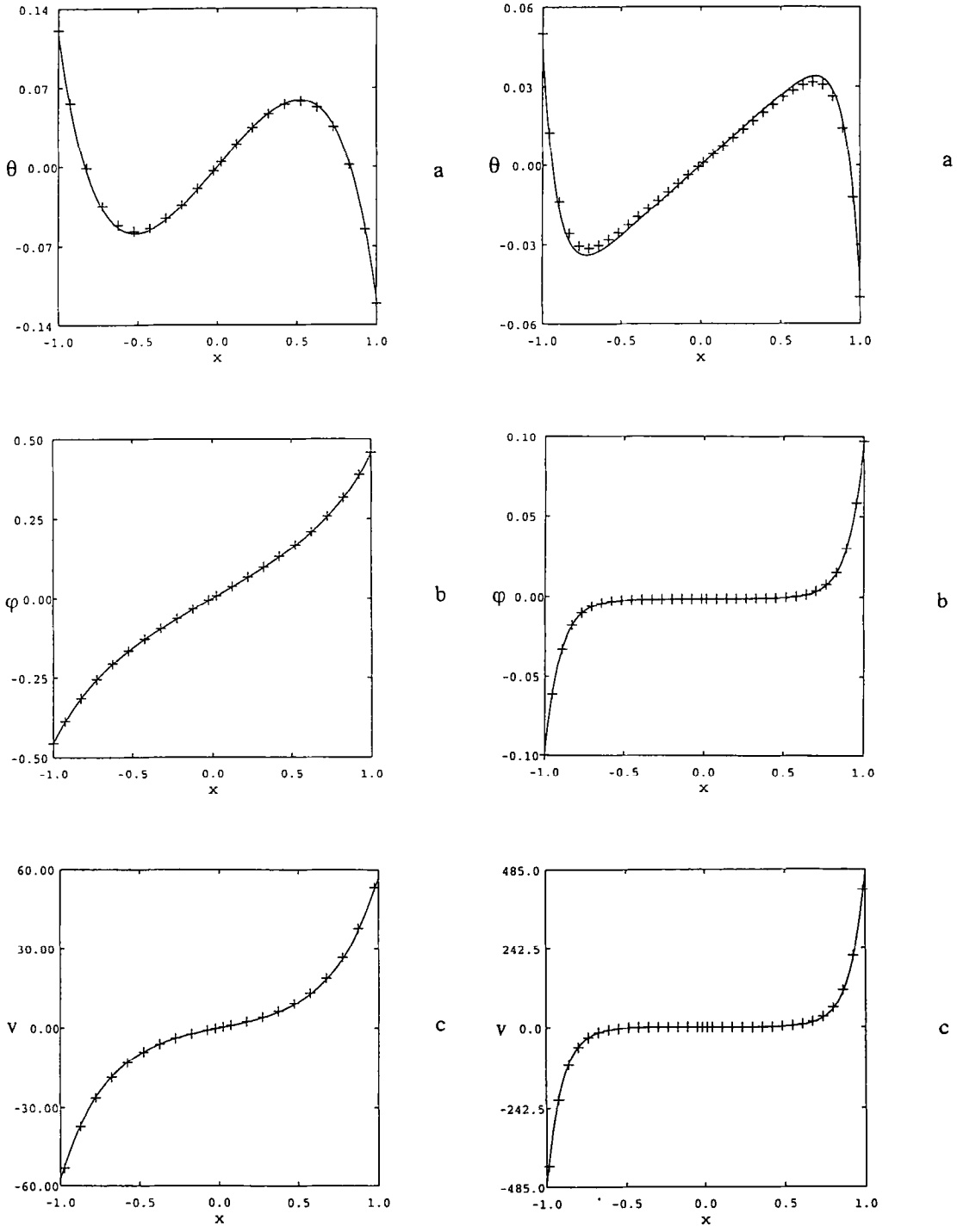

FIG. 9. Comparison between fully numerical (+) and analytical (——) solutions at steady state for $A = 10$, $R_c = 100$, $Le = 10$, $N = 1$ (solute- and heat-driven natural convection), $y = 0$. (a) Concentration, (b) temperature, and (c) velocity.

FIG. 10. Comparison between fully numerical (+) and analytical (——) solutions at steady state for $A = 10$, $R_c = 100$, $Le = 10$, $N = 50$ (heat-driven natural convection), $y = 0$. (a) Concentration, (b) temperature, and (c) velocity.

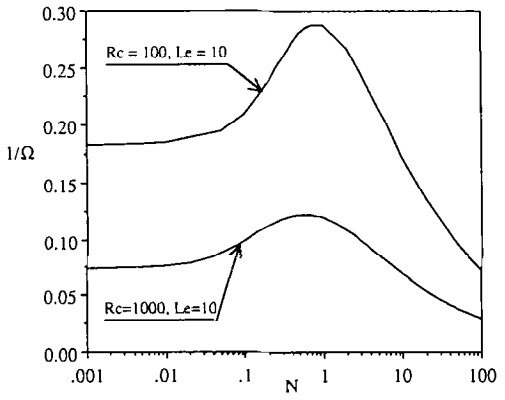

FIG. 11. Variation of the vertical boundary layer thickness with R_c and N.

the thickness of the boundary layers, much like its isosolutal or isothermal counterparts in refs. [4–6], does not vary in the vertical direction, see also Figs. 4(c) and 6(c).

(iii) For given values of R_c and Le, the vertical boundary layer thickness first increases and then decreases as N gradually increases from the limit of solute-driven ($N \ll 1$) to the limit of heat-driven ($N \gg 1$) natural convection. This property is more clearly illustrated in Fig. 11, which also shows that for given values of Le and N, the boundary layer thickness decreases with increasing values of R_c. It should be remarked that the latter occurs in the isothermal and isosolutal counterparts of the present study too and is therefore not a special feature of double diffusive convection.

In most engineering applications, where details of the solution are of less significance, the overall solute and heat transfer rate of the system under consideration is summarized by resorting to Sherwood and Nusselt numbers. In the present analysis, the influence of the various input parameters (R_c, Le, N and A) on the overall behaviour of the system is illustrated by plotting graphs of Sh and Nu versus the input parameters, see Figs. 12 and 13. This approach makes it possible to present large amounts of data within reasonable space and at the same time satisfies interests of engineering applications. Figures 12(a)–(c) show how the overall solute and heat transfer properties of the system respond to increasing R_c, Le and N respectively. The quantity Ω is plotted in the same graphs in order to show the transition to or from boundary layer type solution ($\Omega > 3$). Figure 12(a) shows that for small values of the solutal Rayleigh–Darcy number ($R_c \sim 0.1$), heat and solute transfer is dominated by diffusion. However, as R_c increases, the effect of natural convection first enhances the solute (at $R_c \sim 1$) and then heat transfer (at $R_c \sim 10$) rate of the system. Figure 12(b) illustrates the influence of the Lewis number on the Sherwood and Nusselt numbers. According to Fig. 12(b), for given values of R_c and N,

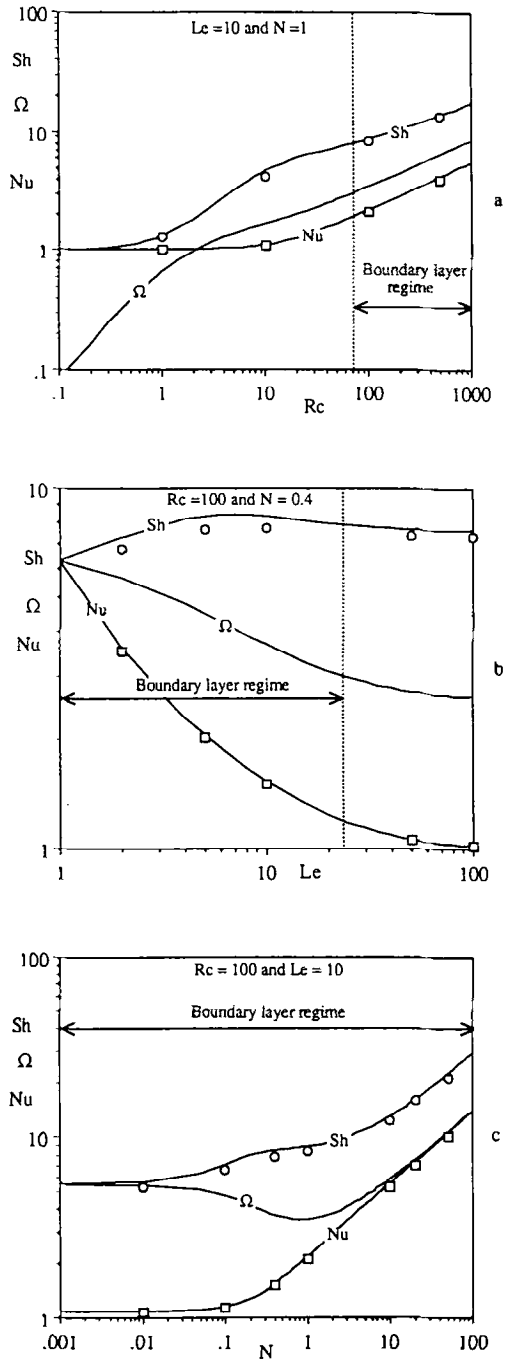

FIG. 12. Comparison between fully numerical (○ : Sherwood number and □ : Nusselt number) and analytical solutions (——) at steady state and for $A = 10$. Influence of (a) solutal Rayleigh–Darcy number R_c, (b) Lewis number Le, and (c) inverse of buoyancy ratio N.

increasing Le leads to a steady decrease of Nu towards the conductive regime while Sh first increases and then decreases asymptotically towards a constant value. Figure 12(b) also shows that an increase in the Lewis number is followed by an increase in the boundary layer thickness ($\delta \sim 1/\Omega$). Figure 12(c) shows that the

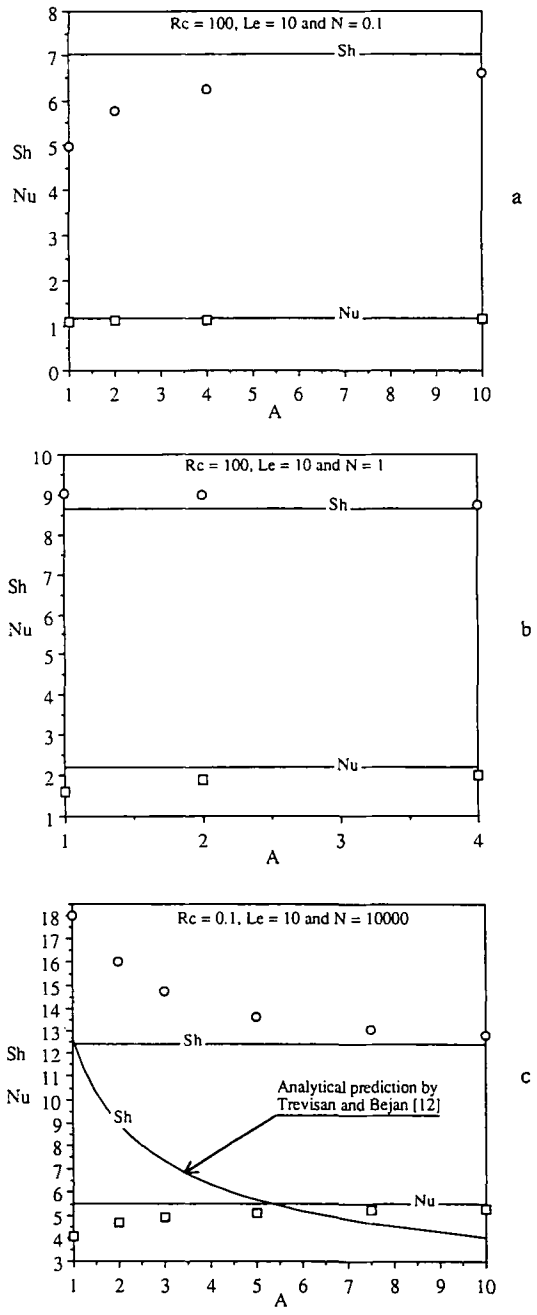

FIG. 13. Comparison between fully numerical (○ : Sherwood number and □ : Nusselt number) and analytical solutions (——) at steady state. Influence of the aspect ratio on (a) solute-driven flow, (b) solute- and heat-driven flow, and (c) heat-driven flow.

Sherwood and Nusselt numbers increase steadily as N increases. Moreover, it shows that in the solute-driven limit, heat transfer is diffusion-dominated and not enhanced by fluid motion while in the heat-driven limit, solute transfer is significantly increased. Note that according to Fig. 12(c), and as predicted by the approximate solutions of Subsections 5.2.3 and 5.2.4, the quantity Ω coincides with the Sherwood number, in the solute-driven limit, and with the Nusselt number, in the heat-transfer limit, respectively.

As already mentioned, the analytical solution is valid if the end effects are confined to small regions adjacent to the top and bottom of the cell. In other words, the enclosure should be tall. The influence of the aspect ratio on the Sherwood and Nusselt numbers is illustrated in Figs. 13(a)–(c). In these Figures, the analytical and numerical solutions are compared for the solute-driven, solute- and heat-driven and heat-driven cases. In the latter case, comparison is also made with the analytical prediction of Sherwood number based on a similarity solution proposed by Trevisan and Bejan [12], see Fig. 13(c). The Figures indicate that the agreement between the analytical solution proposed in this paper and the numerical solution improves as the aspect ratio increases. This can be attributed to three interrelated effects which are brought about by increasing A: (i) shrinking of the end regions relative to the total height of the enclosure, (ii) evolution of the concentration and temperature fields towards the case of linearly stratified fields and (iii) increasing parallelity of the vertical portions of the streamlines. These three effects are better illustrated in Figs. 14–16, which depict the case of comparable thermal and solutal buoyancy forces. Note that according to Fig. 14(a), for $A = 1$, the concentration field is rather uniform in the central parts of the enclosure while it becomes more and more stratified as A increases, see Figs. 14(b) and (c). In the heat-driven limit of convection, the pattern of isosolutes, isotherms and streamlines are qualitatively similar to those of the combined solute- and heat-driven case shown in Figs. 14 and 15. However, in the solute-driven limit, the concentration and temperature fields both are almost linearly, though weakly, stratified even for $A = 1$. It is worth remarking that according to Figs. 14(b) and (c), 15(b) and (c) and 16(b) and (c), which have a weak boundary layer character, the thicknesses of the vertical boundary layers of concentration, temperature and velocity are approximately the same despite the large value of Le. For sufficiently high aspect ratios, the same remark can be made in the solute-driven and heat-driven limits. According to Trevisan and Bejan [12], in the limit of large Lewis numbers: (i) the concentration boundary layer should be much thinner than the velocity boundary layer and (ii) the core of the concentration field should be in a state of almost uniform concentration. However, the results of the present analysis show that these properties prevail only in the solute- and heat-driven, and heat-driven regimes provided that the aspect ratio is not large. It should be added that numerical experiments indicate that the minimum aspect ratio, for and beyond which the analytical solution of Section 5 accurately predicts the corresponding fully numerical solution, increases with increasing the Lewis number.

Last, but not least, the good agreement between the

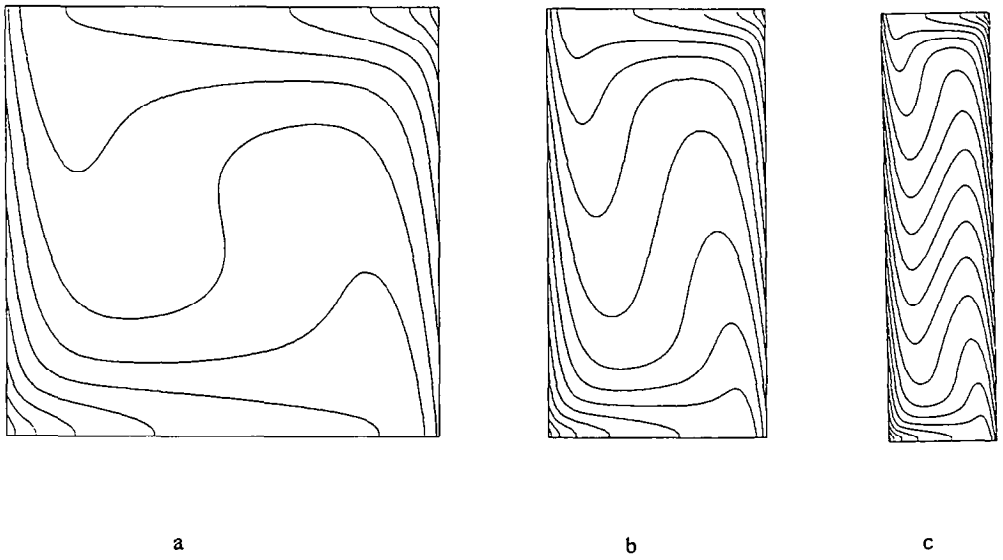

FIG. 14. Influence of increasing the enclosure height (or aspect ratio) on the pattern of isohalines for $R_c = 100$, $Le = 10$, $N = 1$. (a) $A = 1$, $-0.3 \leqslant \theta \leqslant 0.3$ and $\Delta\theta = 0.05$; (b) $A = 2$, $-0.4 \leqslant \theta \leqslant 0.4$ and $\Delta\theta = 0.05$; and (c) $A = 4$, $-0.55 \leqslant \theta \leqslant 0.55$ and $\Delta\theta = 0.05$. θ decreases from the lower left corner to the upper right corner.

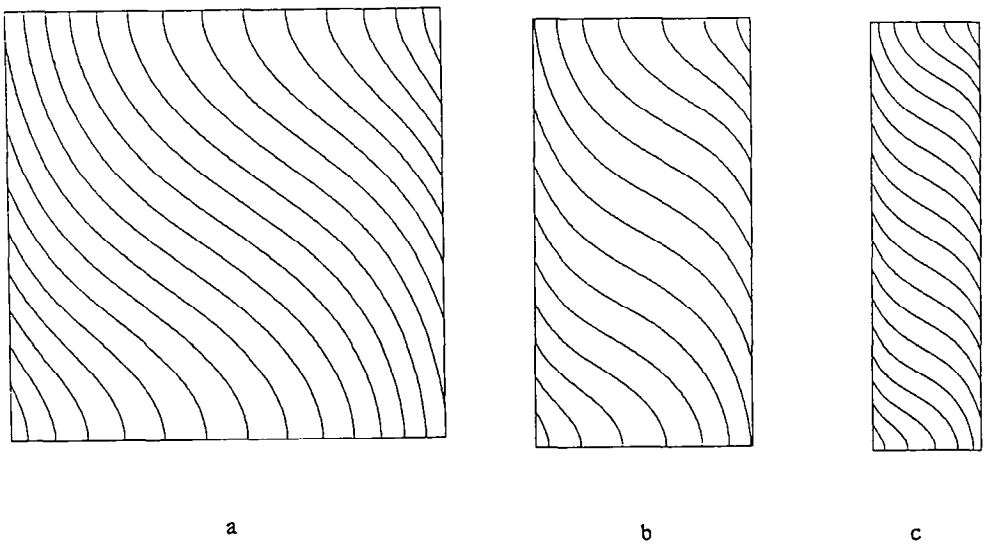

FIG. 15. Influence of increasing the enclosure height (or aspect ratio) on the pattern of isotherms for $R_c = 100$, $Le = 10$, $N = 1$. (a) $A = 1$, $-1 \leqslant \varphi \leqslant 1$ and $\Delta\varphi = 0.1$; (b) $A = 2$, $-1.4 \leqslant \varphi \leqslant 1.4$ and $\Delta\varphi = 0.2$; and (c) $A = 4$, $-2.2 \leqslant \varphi \leqslant 2.2$ and $\Delta\varphi = 0.2$. φ increases from the lower left corner to the upper right corner.

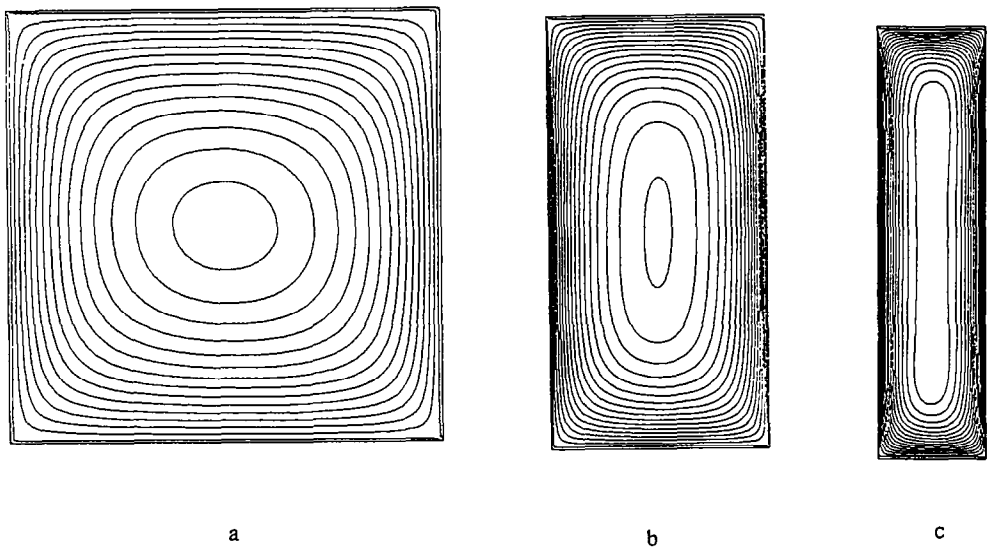

FIG. 16. Influence of increasing the enclosure height (or aspect ratio) on the pattern of streamlines for $R_c = 100$, $Le = 10$, $N = 1$. (a) $A = 1$, $-14 \leqslant \psi \leqslant 0$ and $\Delta\psi = 1$; (b) $A = 2$, $-16 \leqslant \psi \leqslant 0$ and $\Delta\psi = 1$; and (c) $A = 4$, $-1.5 \leqslant \psi \leqslant 0$ and $\Delta\psi = 1$. ψ decreases inwards from the boundaries.

time-consuming numerical solutions and their corresponding analytical solutions, plotted in Figs. 7–10 and 12, proves that the analytical solution presented in Section 5, despite its relative simplicity, is a powerful tool of analysis.

Acknowledgements—The author wishes to thank Dr Shigeo Kimura and Professor Ioan Pop for several illuminating discussions and good comments on the manuscript.

REFERENCES

1. D. A. Nield and A. Bejan, *Convection in Porous Media*, pp. 277–303. Springer, New York (1992).
2. D. J. Tritton, *Physical Fluid Dynamics*, pp. 378–392. Oxford University Press, New York (1988).
3. A. Bejan, The boundary layer regime in a porous layer with uniform heat flux from the side, *Int. J. Heat Mass Transfer* **26**, 1339–1346 (1983).
4. P. Vasseur, M. G. Satish and L. Robillard, Natural convection in a thin inclined porous layer exposed to a constant heat flux, *Heat Transfer*, Vol. 5, pp. 2665–2670. Springer-Verlag, San Francisco (1986).
5. P. Vasseur and L. Robillard, The Brinkman model for boundary layer regime in a rectangular cavity with uniform heat flux from the side, *Int. J. Heat Mass Transfer* **30**, 717–727 (1987).
6. F. Alavyoon, The effects of porous separators on free convection and mass transfer in electrochemical systems—Application to recharging lead-acid cells, *Heat and Mass Transfer in Porous Media*, pp. 349–379. Elsevier, Amsterdam (1992).
7. F. H. Bark, F. Alavyoon and A. A. Dahlkild, On unsteady free convection in vertical slots due to prescribed fluxes of heat or mass at the vertical walls, *J. Fluid Mech.* **235**, 665–689 (1992).
8. F. Alavyoon, A. Eklund, F. H. Bark, R. I. Karlsson and D. Simonsson, Theoretical and experimental studies of free convection and stratification of electrolyte in a lead-acid cell during recharge, *Electrochimica Acta* **14**, 2153–2164 (1991).
9. A. Bejan and K. R. Khair, Heat and mass transfer by natural convection in a porous medium, *Int. J. Heat Mass Transfer* **28**, 909–918 (1985).
10. F. C. Lai and F. A. Kulacki, Coupled heat and mass transfer by natural convection from vertical surfaces in porous media, *Int. J. Heat Mass Transfer* **34**, 1189–1194 (1991).
11. O. V. Trevisan and A. Bejan, Natural convection with combined heat and mass transfer buoyancy effects in porous medium, *Int. J. Heat Mass Transfer* **28**, 1597–1611 (1985).
12. O. V. Trevisan and A. Bejan, Mass and heat transfer by natural convection in a vertical slot filled with porous medium, *Int. J. Heat Mass Transfer* **29**, 403–415 (1986).
13. O. V. Trevisan and A. Bejan, Mass and heat transfer by high Rayleigh number convection in a porous medium heated from below, *Int. J. Heat Mass Transfer* **30**, 2341–2356 (1987).
14. Z. Zhang and A. Bejan, The horizontal spreading of thermal and chemical deposits in a porous medium, *Int. J. Heat Mass Transfer* **30**, 2289–2303 (1987).
15. K. N. Mehta and K. Nandakumar, Natural convection with combined heat and mass transfer buoyancy effects in non-homogeneous porous medium, *Int. J. Heat Mass Transfer* **30**, 2651–2656 (1987).
16. O. V. Trevisan and A. Bejan, Combined heat and mass transfer by natural convection in a porous medium, *Advances in Heat Transfer* **20**, 315–352 (1990).
17. N. D. Rosenberg and F. J. Spera, Thermohaline convection in a porous medium heated from below, *Int. J. Heat Mass Transfer* **35**, 1261–1273 (1992).
18. R. W. Griffiths, Layered double-diffusive convection in porous media, *J. Fluid Mech.* **102**, 221–248 (1981).
19. B. T. Murray and C. F. Chen, Double-diffusive convection in a porous medium, *J. Fluid Mech.* **201**, 147–166 (1989).
20. D. A. Nield, Onset of thermohaline convection in a porous medium, *Water Resour.* **4**, 553–560 (1968).
21. G. Dahlquist and Å. Björck, *Numerical Methods*, p. 172. Prentice-Hall, Engelwood Cliffs, New Jersey (1974).
22. L. Prandtl, *Essentials of fluid dynamics*, p. 442. Blackie, London (1952).
23. O. V. Trevisan and A. Bejan, Combined heat and mass transfer by natural convection in a vertical enclosure, *ASME J. Heat Transfer* **109**, 104–112 (1987).